A Linear Kalman Filter for MARG Orientation Estimation Using the Algebraic Quaternion Algorithm

Roberto G. Valenti, Ivan Dryanovski, and Jizhong Xiao, *Senior Member, IEEE*

***Abstract*— Real-time orientation estimation using low-cost inertial sensors is essential for all the applications where size and power consumption are critical constraints. Such applications include robotics, human motion analysis, and mobile devices. This paper presents a linear Kalman filter for magnetic angular rate and gravity sensors that processes angular rate, acceleration, and magnetic field data to obtain an estimation of the orientation in quaternion representation. Acceleration and magnetic field observations are preprocessed through a novel external algorithm, which computes the quaternion orientation as the composition of two algebraic quaternions. The decoupled nature of the two quaternions makes the roll and pitch components of the orientation immune to magnetic disturbances. The external algorithm reduces the complexity of the filter, making the measurement equations linear. Real-time implementation and the test results of the Kalman filter are presented and compared against a typical quaternion-based extended Kalman filter and a constant gain filter based on the gradient-descent algorithm.**

***Index Terms*— Inertial sensors, Kalman filtering, magnetic sensors, orientation estimation, quaternions.**

I. Introduction

INERTIAL and magnetic sensors are largely used to estimate the orientation of a rigid body with respect to an inertial frame. Their use ranges from aerospace and unmanned vehicles to man–machine iteration and robotics. The development of low-cost and lightweight microelectromechanical systems has allowed smaller and cheaper inertial sensors to be adopted for an even wider range of applications, such as human motion tracking [1], [2], microaerial vehicles [3], [4], and mobile devices [5], [6].

An inertial measurement unit (IMU) is a combination of sensors that typically includes a triaxis accelerometer and triaxis gyroscope. In addition, if the IMU has a triaxis magnetometer, it is referred to as magnetic angular rate and gravity (MARG). The accelerometer observes the IMU's proper acceleration by measuring the weight experienced by a test mass that is at rest in the local sensor frame. When the accelerometer is placed in a gravitational field, and is not subjected to external nongravitational accelerations, it measures the specific force opposing the weight produced by the gravitational pull, and thus, it may be used to infer the magnitude and direction of the gravitational field. Therefore, an accelerometer that is at rest on the surface of the earth measures a vector of magnitude 1 g pointing upward in the local tangent plane coordinate frame.

To obtain an estimation of the orientation, acceleration and magnetic field measurements are fused together with angular rate readings from the gyroscope by means of a specific orientation estimation algorithm. Many approaches have been studied for this purpose. We can classify them into two categories depending on whether they use a stochastic approach or a frequency analysis. Among the stochastic approaches, Kalman filter-based techniques are by far the most common ones. They adopt a probabilistic determination of the state modeled as a Gaussian distribution given the system's model. They are widely used in aerospace applications [7], [8], human motion analysis [9]–[11], and robotics [12], [13]. Filters based on frequency analysis are a common alternative to Kalman filter (KFs) because of their simplicity and effectiveness. Complementary observers [14]–[16] and other constant gain filters [17] use an analysis in the frequency domain to filter the signals coming from different sources and combine them together to obtain a more accurate orientation estimation without any statistical description. A typical drawback of a constant gain filter is the inability to adapt the weight of the different sources of information when their accuracy is affected. More recent filters address this problem by adopting an adaptive gain algorithm [18]–[20], which automatically changes the gain value according to the perceived external conditions, such as nongravitational acceleration and magnetic disturbances. A survey of other nonlinear estimation methods can be found in [21].

Most of the recent sensor fusion algorithms for inertial/magnetic sensors provide an orientation estimation in quaternion form. Unlike Euler angles, quaternions do not suffer from the singularity configuration known as the gimbal lock. Among all the orientation representations that avoid the gimbal lock, quaternions have the minimal number of parameters, hence requiring less computation time. Furthermore, the quaternion representation offers a linear formulation of the orientation dynamics and rotations of vectors are simply performed by quaternion multiplications.

Manuscript received May 20, 2015; revised September 18, 2015; accepted September 19, 2015. Date of publication December 3, 2015; date of current version January 4, 2016. This work was supported in part by the U.S. Army Research Office under Grant W911NF-09-1-0565 and in part by the U.S. National Science Foundation under Grant IIS-0644127 and Grant CBET-1160046. The Associate Editor coordinating the review process was Dr. Huang-Chen Lee. *(Corresponding author: Jizhong Xiao.)*

R. G. Valenti and J. Xiao are with the Department of Electrical Engineering, The City College of New York, New York, NY 10031 USA (e-mail: rvalent00@citymail.cuny.edu; jxiao@ccny.cuny.edu).

I. Dryanovski is with the Department of Computer Science, The Graduate Center, The City University of New York, New York, NY 10016 USA (e-mail: idryanovski@gc.cuny.edu).

Color versions of one or more of the figures in this paper are available online at http://ieeexplore.ieee.org.

Digital Object Identifier 10.1109/TIM.2015.2498998

The extended Kalman filter is the basis of IMU-based orientation estimations. It can be implemented such that the state includes the orientation components for a direct orientation estimation or with the state composed of the orientation error whose estimation will be used to indirectly obtain the final orientation. These two KF approaches are referred to as direct extended Kalman filter(EKF) and indirect EKF. If the orientation is expressed in quaternion form, the direct and indirect EKFs are commonly known as additive EKF (AEKF) and multiplicative EKF (MEKF), respectively, due to the quaternion error form that distinguishes each case. A discussion about the differences between the two methods can be found in [22].

In their first approach, Marins *et al.* [9] present an AEKF to estimate the orientation in quaternion form and the angular velocity vector from a MARG sensor. Sabatini [10] directly estimates the quaternion orientation adopting an EKF, which is also used to estimate accelerometer and magnetometer biases by state augmentation for online calibration. Sabatini [24] presents an EKF where the state, composed of the quaternion components, is augmented with magnetic distortion vector, modeled as a Gauss–Markov process, to reduce the heading drift in magnetically nonhomogeneous environments. Moreover, the author presents the observability analysis of the filter. Zhang *et al.* [25] propose a quaternion-based Kalman filter, which adopts a linear process and measurement model thanks to the manipulation of acceleration and magnetometer readings to establish the linear pseudomeasurement equation. Such a linear KF is able to deal with temporary external interference such as nongravitational acceleration and magnetic disturbances by means of a vector selection scheme based on the predicted measurement.

Trawny and Roumeliotis [26] present an indirect EKF where the error vector is expressed as the small rotation between the estimated and the true orientation of the local frame of reference and is defined as a quaternion multiplication (from here the term multiplicative). This approach reduces the size of the state vector and avoids any possible instability of the error covariance. A similar approach is adopted in the MEKF in [27]. Suh [28] proposes a quaternion-based indirect Kalman filter with a two-step measurement update and adaptive estimation of external acceleration. The two-step measurement update consists of an accelerometer measurement update and a magnetic sensor measurement update. The two updates are decoupled such that acceleration data are used only to update roll and pitch components of the orientation, while the second step uses only magnetometer measurements to correct the yaw. Therefore, magnetic disturbances will not affect the roll and pitch. Because of the separation of the measurement update equation into two stages, the algorithm is rather complicated. Hence, Suh *et al.* [29] propose a new measurement equation for the quaternion-based indirect Kalman filter, where roll and pitch are only slightly affected by the magnetic sensor.

To reduce the complexity of a quaternion-based EKF and avoid the linearization procedure, which might reduce the convergence rate and introduce approximation errors, a two-layer filter architecture can be adopted. The first layer is dedicated to an external algorithm to evaluate the quaternion orientation from acceleration and magnetic field data by solving the Wahba's problem [30]. The second layer is a linear Kalman filter that applies the quaternion output of the first layer as the input of the measurement process. This strategy has been applied by many researchers using different external estimators of the quaternion orientation. Marins *et al.* [9], in their second approach, and Yun *et al.* [23] use a Gauss–Newton optimization algorithm. Yun and Bachmann [31] apply the quaternion estimator (QUEST) [32], and Seo *et al.* [33] use the factored quaternion algorithm (FQA) [34]. The main difference between these methods is the computational speed of the external QUEST. Most of these methods find the quaternion orientation as output of a minimization technique by minimizing a cost function through a sequence of iterations. Usually, in KF applications, only one iteration is used because generally the rate of convergence of the optimization algorithm is higher than the angular speed. However, when the orientation variation rate increases, the optimization algorithm reduces its performance, adding error to the estimate produced by the filter. The FQA computes the orientation of a rigid body based on earth gravity and magnetic field measurements. The quaternion orientation is estimated by analyzing a series of three sequential rotations. This approach reduces the orientation error caused by the presence of local magnetic disturbances, only into the error in the yaw component maintaining the accuracy of the QUEST algorithm. Nevertheless, the FQA is computationally more efficient than QUEST by about 25% [34].

In this paper, we describe a linear Kalman filter using the two-layer structure described above, adopting a novel external QUEST. The novel algorithm finds a quaternion orientation by solving Whaba's problem through the processing of gravity and magnetic field observations. Unlike the FQA, the presented method computes the orientation as a sequence of only two rotations. The first rotation defines a tilt quaternion, giving information about the roll and pitch angles, while the second heading quaternion contains the yaw angle. Both quaternions are found as an algebraic solution of a system instead of the result of an optimization problem. By construction, the output quaternion does not suffer from singularity states; moreover, the heading quaternion, which is found by processing magnetic field data, does not change the bearing information contained in the tilt quaternion. Therefore, in the case of magnetic disturbances that alter the reference direction of the magnetic north, the error will affect only the yaw angle.

Furthermore, we derive the covariance matrix of the orientation quaternion via propagation of the acceleration and magnetic field's standard deviations. To accomplish this, we approximate the quaternion as a normally distributed random vector. This derivation facilitates the use of the quaternion as the correction measurement in the Kalman filter framework.

II. Background Theory

Any arbitrary orientation in the 3-D space of frame A with respect to frame B can be represented by a unit quaternion ${}^{B}_{A}\boldsymbol{q}$

defined as follows:

$$ {}^{B}_{A}\boldsymbol{q} = \begin{bmatrix} q_0 \\ q_1 \\ q_2 \\ q_3 \end{bmatrix} = \begin{bmatrix} \cos\dfrac{\alpha}{2} \\ e_x \sin\dfrac{\alpha}{2} \\ e_y \sin\dfrac{\alpha}{2} \\ e_z \sin\dfrac{\alpha}{2} \end{bmatrix} \tag{1} $$

where α is the rotation angle and $\boldsymbol{e}$ is the unit vector that represents the rotation axis. The quaternion conjugate of ${}^{B}_{A}\boldsymbol{q}$, given its unit norm, is equivalent to the inverse quaternion and describes the inverse rotation. Therefore, the conjugate quaternion can be used to represent the orientation of frame B relative to frame A, as defined in the following:

$$ {}^{B}_{A}\boldsymbol{q}^{*} = {}^{A}_{B}\boldsymbol{q} = \begin{bmatrix} q_0 \\ -q_1 \\ -q_2 \\ -q_3 \end{bmatrix}. \tag{2} $$

The orientation quaternion after a sequence of rotations can be easily found by quaternion multiplication where each quaternion represents the orientation of a frame with respect to the rotated one. For example, given three frames A, B, and C, and given the quaternion ${}^{B}_{A}\boldsymbol{q}$ orientation of frame A expressed with respect to frame B, and given the quaternion ${}^{C}_{B}\boldsymbol{q}$ orientation of frame B expressed with respect to frame C, the orientation of frame A with respect to frame C is characterized by

$$ {}^{C}_{A}\boldsymbol{q} = {}^{C}_{B}\boldsymbol{q} \otimes {}^{B}_{A}\boldsymbol{q} \tag{3} $$

where quaternion multiplication, given two quaternions $\boldsymbol{p}$ and $\boldsymbol{q}$, is defined as

$$ \boldsymbol{p} \otimes \boldsymbol{q} = \begin{bmatrix} p_0q_0 - p_1q_1 - p_2q_2 - p_3q_3 \\ p_0q_1 + p_1q_0 + p_2q_3 - p_3q_2 \\ p_0q_2 - p_1q_3 + p_2q_0 + p_3q_1 \\ p_0q_3 + p_1q_2 - p_2q_1 + p_3q_0 \end{bmatrix}. \tag{4} $$

Unit quaternions can be applied to operate rotations of 3-D vectors. For example, vector ${}^{A}\boldsymbol{v}$, expressed with respect to frame A, can be expressed with respect to frame B by the following operation:

$$ {}^{B}\boldsymbol{v}_q = {}^{B}_{A}\boldsymbol{q} \otimes {}^{A}\boldsymbol{v}_q \otimes {}^{B}_{A}\boldsymbol{q}^{*} \tag{5} $$

where the symbol $\otimes$ indicates the quaternion multiplication, and ${}^{A}\boldsymbol{v}_q$ and ${}^{B}\boldsymbol{v}_q$ are the observations of vector $\boldsymbol{v}$, in the two reference frames, written as pure quaternions as shown in

$$ \boldsymbol{v}_q = \begin{bmatrix} 0 \\ \boldsymbol{v} \end{bmatrix} = \begin{bmatrix} 0 \\ v_x \\ v_y \\ v_z \end{bmatrix}. \tag{6} $$

The inverse rotation that describes vector ${}^{B}\boldsymbol{v}$ relative to frame A can be easily found using the property of the conjugate quaternion, and it is presented in

$$ {}^{A}\boldsymbol{v}_q = {}^{B}_{A}\boldsymbol{q}^{*} \otimes {}^{B}\boldsymbol{v}_q \otimes {}^{B}_{A}\boldsymbol{q} = {}^{A}_{B}\boldsymbol{q} \otimes {}^{B}\boldsymbol{v}_q \otimes {}^{A}_{B}\boldsymbol{q}^{*}. \tag{7} $$

The rotation defined in (5) can be written in matrix form as in

$$ {}^{B}\boldsymbol{v} = \mathbf{R}\left({}^{B}_{A}\boldsymbol{q}\right){}^{A}\boldsymbol{v} \tag{8} $$

where $\mathbf{R}\left({}^{B}_{A}\boldsymbol{q}\right)$, which belongs to the 3-D special orthogonal group SO(3), is the direct cosine matrix given in terms of the orientation quaternion ${}^{B}_{A}\boldsymbol{q}$ as shown in the following:

$$ \begin{bmatrix} q_0^2 + q_1^2 - q_2^2 - q_3^2 & 2(q_1q_2 - q_0q_3) & 2(q_1q_3 + q_0q_2) \\ 2(q_1q_2 + q_0q_3) & q_0^2 - q_1^2 + q_2^2 - q_3^2 & 2(q_2q_3 - q_0q_1) \\ 2(q_1q_3 - q_0q_2) & 2(q_2q_3 + q_0q_1) & q_0^2 - q_1^2 - q_2^2 + q_3^2 \end{bmatrix}. \tag{9} $$

Given the properties of the elements of SO(3), the inverse rotation can be defined as

$$ {}^{A}\boldsymbol{v} = \mathbf{R}\left({}^{A}_{B}\boldsymbol{q}\right){}^{B}\boldsymbol{v} = \mathbf{R}^{\mathsf{T}}\left({}^{B}_{A}\boldsymbol{q}\right){}^{B}\boldsymbol{v}. \tag{10} $$

III. Algebraic Quaternion Algorithm

In this section, we analyze the algebraic derivation of a quaternion from the observation of the earth's fields. For a clear understanding of the following derivation, let us first define a notation that will be used throughout this paper. We refer to the local (sensor) frame as L and the global (earth) frame as G. We can define the measured acceleration ${}^{L}\boldsymbol{a}$ and the true earth gravitational acceleration ${}^{G}\boldsymbol{g}$ as the unit vectors

$$ {}^{L}\boldsymbol{a} = [\, a_x \quad a_y \quad a_z \,]^{\mathsf{T}}, \quad \|\boldsymbol{a}\| = 1 $$
$$ {}^{G}\boldsymbol{g} = [\, 0 \quad 0 \quad 1 \,]^{\mathsf{T}}. $$

Similarly, we define the measured local magnetic field ${}^{L}\boldsymbol{m}$ and the true magnetic field ${}^{G}\boldsymbol{h}$ as the unit vectors

$$ {}^{L}\boldsymbol{m} = [\, m_x \quad m_y \quad m_z \,]^{\mathsf{T}}, \quad \|\boldsymbol{m}\| = 1 $$
$$ {}^{G}\boldsymbol{h} = [\, h_x \quad h_y \quad h_z \,]^{\mathsf{T}}, \quad \|\boldsymbol{h}\| = 1. $$

Finally, the gyroscopes measure the angular velocity ${}^{L}\boldsymbol{\omega}$ around the three sensor frame axes

$$ {}^{L}\boldsymbol{\omega} = [\, \omega_x \quad \omega_y \quad \omega_z \,]^{\mathsf{T}}. $$

Note that most IMUs usually measure nonnormalized vectors $\boldsymbol{a}$ and $\boldsymbol{m}$. However, for the purposes of derivation in this paper, we assume that the quantities have been normalized. The only relevant units are those of $\boldsymbol{\omega}$, which we assume are radians per second.

We present an algebraic derivation of the orientation quaternion ${}^{L}_{G}\boldsymbol{q}$, of the global frame (G) relative to the local frame (L), as a function of ${}^{L}\boldsymbol{a}$ and ${}^{L}\boldsymbol{m}$. We have two independent sensors observing two independent fields; a straightforward way to formulate the quaternion is through the inverse orientation that rotates the measured quantities ${}^{L}\boldsymbol{a}$ and ${}^{L}\boldsymbol{m}$ into the reference quantities ${}^{G}\boldsymbol{g}$ and ${}^{G}\boldsymbol{h}$

$$ \begin{cases} \mathbf{R}^{\mathsf{T}}\left({}^{L}_{G}\boldsymbol{q}\right){}^{L}\boldsymbol{a} = {}^{G}\boldsymbol{g} \\ \mathbf{R}^{\mathsf{T}}\left({}^{L}_{G}\boldsymbol{q}\right){}^{L}\boldsymbol{m} = {}^{G}\boldsymbol{h}. \end{cases} \tag{11} $$

This system, however, is overdetermined—each of the two equations provides two independent constraints on the orientation ${}^{L}_{G}\boldsymbol{q}$, whereas the orientation has only three degrees

of freedom. In the case when there is a disagreement between the gravitational and magnetometer readings, the system will not have a solution. The disagreement could arise from random sensor noise or unmodeled field disturbances (nongravitational accelerations or magnetic field variations). A possible solution would be to define an error metric and find the quaternion that minimizes this error. However, this could still result in disturbances in the magnetic field affecting the roll and pitch, which we are trying to avoid.

To address this problem, we present a modified system of equations. The definition of the system (but not its solution) is based on the approach presented in [17]. First, we redefine the global coordinate frame G to be aligned with the magnetic north. Specifically, the global frame's x-axis points in the same direction as the local magnetic field (the z-axis remains vertical). Obviously, this global frame is fixed only in the case when the local magnetic field does not change its heading.

Next, we modify the system in (11) so that the second equation provides only one constraint. Let ${}^{G}\Pi_{zx^+}$ be the half-plane that contains all points that lie in the global xz plane such that x is nonnegative. We require that the magnetic reading, when rotated into the global frame, lies on the half-plane ${}^{G}\Pi_{zx^+}$. Thus, we guarantee that the heading will be measured with respect to magnetic north, but do not enforce a constraint on the magnetic inclination

$$\begin{cases} \mathbf{R}^{\mathsf{T}}\left({}^{L}_{G}\boldsymbol{q}\right){}^{L}\boldsymbol{a} = {}^{G}\boldsymbol{g} \\ \mathbf{R}^{\mathsf{T}}\left({}^{L}_{G}\boldsymbol{q}\right){}^{L}\boldsymbol{m} \in {}^{G}\Pi_{zx^+}. \end{cases} \tag{12}$$

Note that when defined in this manner, the system no longer needs *a priori* knowledge of the direction of the earth's magnetic field ${}^{G}\boldsymbol{h}$.

In the remainder of the section, we present a novel algebraic solution to obtain ${}^{L}_{G}\boldsymbol{q}$ as a function of ${}^{L}\boldsymbol{a}$ and ${}^{L}\boldsymbol{m}$. We begin by decomposing ${}^{L}_{G}\boldsymbol{q}$ into two auxiliary quaternions: ${}^{L}_{I}\boldsymbol{q}_{\text{acc}}$ and ${}^{I}_{G}\boldsymbol{q}_{\text{mag}}$. The quaternion ${}^{L}_{I}\boldsymbol{q}_{\text{acc}}$ can be defined as the orientation of an intermediate frame (I), the z-axis of which coincides with the z-axis of the global frame and with different unknown x and y axes, with respect to the local frame. The quaternion ${}^{I}_{G}\boldsymbol{q}_{\text{mag}}$ represents the orientation of the global frame relative to the intermediate frame. Finally, we can write the quaternion ${}^{L}_{G}\boldsymbol{q}$ as

$${}^{L}_{G}\boldsymbol{q} = {}^{L}_{I}\boldsymbol{q}_{\text{acc}} \otimes {}^{I}_{G}\boldsymbol{q}_{\text{mag}} \tag{13}$$

and

$$\mathbf{R}\left({}^{L}_{G}\boldsymbol{q}\right) = \mathbf{R}\left({}^{L}_{I}\boldsymbol{q}_{\text{acc}}\right)\mathbf{R}\left({}^{I}_{G}\boldsymbol{q}_{\text{mag}}\right). \tag{14}$$

We further define ${}^{I}_{G}\boldsymbol{q}_{\text{mag}}$ to have only a single degree of freedom, by setting it to

$${}^{I}_{G}\boldsymbol{q}_{\text{mag}} = \begin{bmatrix} q_{0_{\text{mag}}} \\ 0 \\ 0 \\ q_{3_{\text{mag}}} \end{bmatrix}. \tag{15}$$

It follows from the quaternion definition in (1) that ${}^{I}_{G}\boldsymbol{q}_{\text{mag}}$ represents a rotation around the z-axis only. In order to keep a simpler notation of the quaternions, from now on, we will omit the reference frames of $\boldsymbol{q}_{\text{acc}}$ and $\boldsymbol{q}_{\text{mag}}$.

In the following sections, we present an algebraic derivation of $\boldsymbol{q}_{\text{acc}}$ and $\boldsymbol{q}_{\text{mag}}$.

A. Quaternion From Accelerometer Readings ($\boldsymbol{q}_{acc}$)

In this section, we present a derivation for the auxiliary quaternion $\boldsymbol{q}_{\text{acc}}$ as a function of ${}^{L}\boldsymbol{a}$. The observations of the gravity vector in the two reference frames allow us to find the quaternion that performs the transformation between the two representations. The rotation in the first equation of system (12) can be rewritten as

$$\mathbf{R}\left({}^{L}_{G}\boldsymbol{q}\right){}^{G}\boldsymbol{g} = {}^{L}\boldsymbol{a} \tag{16}$$

and decomposed using (14) obtaining

$$\mathbf{R}(\boldsymbol{q}_{\text{acc}})\mathbf{R}(\boldsymbol{q}_{\text{mag}}) \begin{bmatrix} 0 \\ 0 \\ 1 \end{bmatrix} = \begin{bmatrix} a_x \\ a_y \\ a_z \end{bmatrix}. \tag{17}$$

The representation of the gravity vector in the global frame has a component only on the z-axis; therefore, any rotation about this axis does not produce any change on it. Consequently, (17) is equivalent to

$$\mathbf{R}(\boldsymbol{q}_{\text{acc}}) \begin{bmatrix} 0 \\ 0 \\ 1 \end{bmatrix} = \begin{bmatrix} a_x \\ a_y \\ a_z \end{bmatrix}. \tag{18}$$

Expanding the multiplication, we obtain the following system:

$$\begin{cases} 2(q_{1_{\text{acc}}}q_{3_{\text{acc}}} + q_{0_{\text{acc}}}q_{2_{\text{acc}}}) = a_x \\ 2(q_{2_{\text{acc}}}q_{3_{\text{acc}}} - q_{0_{\text{acc}}}q_{1_{\text{acc}}}) = a_y \\ q^2_{0_{\text{acc}}} - q^2_{1_{\text{acc}}} - q^2_{2_{\text{acc}}} + q^2_{3_{\text{acc}}} = a_z. \end{cases} \tag{19}$$

It is clear that the above system is underdetermined and has an infinite number of solutions. This is not an unexpected result because the alignment of the gravity vector from its representation in the global frame into the local frame does not give any information about the rotation around the z-axis (yaw). Thus, such an alignment can be achieved by infinite rotations with definite roll and pitch angles and arbitrary yaw. To restrict the solutions to a finite number, we choose $q_{3_{\text{acc}}} = 0$ simplifying system (19) to

$$\begin{cases} 2q_{0_{\text{acc}}}q_{2_{\text{acc}}} = a_x \\ -2q_{0_{\text{acc}}}q_{1_{\text{acc}}} = a_y \\ q^2_{0_{\text{acc}}} - q^2_{1_{\text{acc}}} - q^2_{2_{\text{acc}}} = a_z. \end{cases} \tag{20}$$

The above system is fully determined; solving it results in four solutions for $\boldsymbol{q}_{\text{acc}}$. Two can be discarded since they have a negative norm. The remaining two are equivalent, with all the quaternion elements switching signs between one solution and the other. For convenience, we choose the solution with positive quaternion scalar (q_0), which corresponds to the shortest path quaternion formulation [35]. Thus, we get

$$\boldsymbol{q}_{\text{acc}} = \begin{bmatrix} \lambda_1 & -\dfrac{a_y}{2\lambda_1} & \dfrac{a_x}{2\lambda_1} & 0 \end{bmatrix}^{\mathsf{T}}, \quad \lambda_1 = \sqrt{\frac{a_z + 1}{2}}. \tag{21}$$

The formulation in (21) is valid for all values of a_z except $a_z = -1$ in which it has a singularity. Furthermore, numerical instability may arise when in proximity to the singularity point.

To address this issue, we provide an alternative solution to system (19). By simply setting $q_{2_{\text{acc}}} = 0$ instead of $q_{3_{\text{acc}}} = 0$ in (19), we obtain the reduced system

$$\begin{cases} 2q_{1_{\text{acc}}}q_{3_{\text{acc}}} = a_x \\ 2q_{0_{\text{acc}}}q_{1_{\text{acc}}} = a_y \\ q_{0_{\text{acc}}}^2 - q_{1_{\text{acc}}}^2 - q_{3_{\text{acc}}}^2 = a_z \end{cases} \tag{22}$$

which admits two real solutions and the following is the one we choose:

$$\boldsymbol{q}_{\text{acc1}} = \begin{bmatrix} -\dfrac{a_y}{2\lambda_2} & \lambda_2 & 0 & \dfrac{a_x}{2\lambda_2} \end{bmatrix}^{\mathsf{T}}, \quad \lambda_2 = \sqrt{\frac{1-a_z}{2}}. \tag{23}$$

This formulation for $\boldsymbol{q}_{\text{acc}}$ has a singularity at $a_z = 1$. Therefore, the final formulation of $\boldsymbol{q}_{\text{acc}}$ that avoids the singularity problem can be obtained by combining (21) and (23)

$$\boldsymbol{q}_{\text{acc}} = \begin{cases} \begin{bmatrix} \lambda_1 & -\dfrac{a_y}{2\lambda_1} & \dfrac{a_x}{2\lambda_1} & 0 \end{bmatrix}^{\mathsf{T}}, & a_z \geq 0 \\ \begin{bmatrix} -\dfrac{a_y}{2\lambda_2} & \lambda_2 & 0 & \dfrac{a_x}{2\lambda_2} \end{bmatrix}^{\mathsf{T}}, & a_z < 0. \end{cases} \tag{24}$$

Effectively, we solve the singularity problem by having two separate formulations for $\boldsymbol{q}_{\text{acc}}$ depending on the hemisphere in which $\boldsymbol{a}$ is pointing. Note that, defined in this manner, $\boldsymbol{q}_{\text{acc}}$ is not continuous at the $a_z = 0$ point. However, we will demonstrate that this problem is resolved with the formulation of $\boldsymbol{q}_{\text{mag}}$ in the following section.

B. Quaternion From Magnetometer Readings ($\boldsymbol{q}_{mag}$)

In this section, we present a derivation for the auxiliary quaternion $\boldsymbol{q}_{\text{mag}}$ as a function of ${}^{L}\boldsymbol{m}$ and $\boldsymbol{q}_{\text{acc}}$. First, we use the quaternion $\boldsymbol{q}_{\text{acc}}$ to rotate the body frame magnetic field vector ${}^{L}\boldsymbol{m}$ into an intermediate frame whose z-axis is the same as the global coordinate frame with orthogonal x and y axes pointing in unknown directions due to the unknown yaw of $\boldsymbol{q}_{\text{acc}}$

$$\mathbf{R}^{\mathsf{T}}(\boldsymbol{q}_{\text{acc}})^{L}\boldsymbol{m} = \boldsymbol{l} \tag{25}$$

where $\boldsymbol{l}$ is the rotated magnetic field vector. Next, we find the quaternion ($\boldsymbol{q}_{\text{mag}}$) that rotates vector $\boldsymbol{l}$ into the vector that lies on the ${}^{G}\Pi_{zx^+}$ of (12) using the following system:

$$\mathbf{R}^{\mathsf{T}}(\boldsymbol{q}_{\text{mag}}) \begin{bmatrix} l_x \\ l_y \\ l_z \end{bmatrix} = \begin{bmatrix} \sqrt{\Gamma} \\ 0 \\ l_z \end{bmatrix} \tag{26}$$

where

$$\Gamma = l_x^2 + l_y^2. \tag{27}$$

This quaternion performs a rotation only about the global z-axis by aligning the x-axis of the intermediate frame into the positive direction of the magnetic north pole, which coincides with the x-direction of our global frame. This rotation will change only the heading component of the orientation without affecting the roll and pitch components. Therefore, when magnetic disturbances are present, their influence is only limited on affecting the heading angle. The quaternion $\boldsymbol{q}_{\text{mag}}$ has the following form:

$$\boldsymbol{q}_{\text{mag}} = \begin{bmatrix} q_{0_{\text{mag}}} & 0 & 0 & q_{3_{\text{mag}}} \end{bmatrix}^{\mathsf{T}}. \tag{28}$$

By reordering system (26) and substituting $\boldsymbol{q}_{\text{mag}}$ with its components, we find the following simplified system:

$$\begin{cases} \left(q_{0_{\text{mag}}}^2 - q_{0_{\text{mag}}}^2\right)\sqrt{\Gamma} = l_x \\ 2q_{0_{\text{mag}}}q_{3_{\text{mag}}}\sqrt{\Gamma} = l_y \\ \left(q_{0_{\text{mag}}}^2 + q_{3_{\text{mag}}}^2\right)l_z = l_z. \end{cases} \tag{29}$$

The solution of the above system that ensures the shortest rotation is the following:

$$\boldsymbol{q}_{\text{mag}} = \begin{bmatrix} \dfrac{\sqrt{\Gamma + l_x\sqrt{\Gamma}}}{\sqrt{2\Gamma}} & 0 & 0 & \dfrac{l_y}{\sqrt{2}\sqrt{\Gamma + l_x\sqrt{\Gamma}}} \end{bmatrix}^{\mathsf{T}}. \tag{30}$$

When the z-component of the local frame acceleration is negative, the local magnetic field vector $\boldsymbol{m}$ is projected onto the horizontal plane using the $\boldsymbol{q}_{\text{acc}}$ formulation of (23). This formulation of $\boldsymbol{q}_{\text{acc}}$ not only projects $\boldsymbol{m}$ onto the horizontal plane, obtaining $\boldsymbol{l}$, but also performs a 180° rotation about the global z-axis, leading into a negative l_x component. It is clear from the formulation of $\boldsymbol{q}_{\text{mag}}$ that the latter quaternion incurs in a singularity state for negative l_x and zero l_y. To avoid the singularity of $\boldsymbol{q}_{\text{mag}}$, we prevent the $\boldsymbol{l}$ vector from having negative x-component by rotating it 180° around the world z-frame, applying the quaternion $\boldsymbol{q}_{\pi} = \begin{bmatrix} 0 & 0 & 0 & 1 \end{bmatrix}^{\mathsf{T}}$. Finally, the rotated vector is used to find $\boldsymbol{q}_{\text{mag}^+}$, which has the same form of (30) and aligns $\boldsymbol{l}$ with the magnetic north. The sequences of rotations are summarized in the quaternion multiplications

$$\boldsymbol{q}_{\text{mag}^+}^{*} \otimes \boldsymbol{q}_{\pi}^{*} \otimes \boldsymbol{q}_{\text{acc}}^{*} \otimes \boldsymbol{m}_q \otimes \boldsymbol{q}_{\text{acc}} \otimes \boldsymbol{q}_{\pi} \otimes \boldsymbol{q}_{\text{mag}^+} \tag{31}$$

where $\boldsymbol{m}_q$ is the local magnetic field vector written as pure quaternion and $\boldsymbol{q}_{\text{acc}}^{*} \otimes \boldsymbol{m}_q \otimes \boldsymbol{q}_{\text{acc}} = \boldsymbol{l}_q$. For the sake of simplicity, we consider the quaternion product between $\boldsymbol{q}_{\pi}$ and $\boldsymbol{q}_{\text{mag}^+}$ as the alternative formulation of $\boldsymbol{q}_{\text{mag}}$ in the case of $l_x < 0$ as follows:

$$\boldsymbol{q}_{\text{mag}} = \boldsymbol{q}_{\pi} \otimes \boldsymbol{q}_{\text{mag}^+}. \tag{32}$$

The result of the above multiplication is shown in

$$\boldsymbol{q}_{\text{mag}} = \begin{bmatrix} \dfrac{l_y}{\sqrt{2}\sqrt{\Gamma - l_x\sqrt{\Gamma}}} & 0 & 0 & \dfrac{\sqrt{\Gamma - l_x\sqrt{\Gamma}}}{\sqrt{2\Gamma}} \end{bmatrix}^{\mathsf{T}}. \tag{33}$$

The complete formulation of $\boldsymbol{q}_{\text{mag}}$ that avoids the singularity problem discussed above is eventually obtained by combining (30) with (33)

$$\boldsymbol{q}_{\text{mag}} = \begin{cases} \begin{bmatrix} \dfrac{\sqrt{\Gamma + l_x\sqrt{\Gamma}}}{\sqrt{2\Gamma}} & 0 & 0 & \dfrac{l_y}{\sqrt{2}\sqrt{\Gamma + l_x\sqrt{\Gamma}}} \end{bmatrix}^{\mathsf{T}}, & l_x \geq 0 \\ \begin{bmatrix} \dfrac{l_y}{\sqrt{2}\sqrt{\Gamma - l_x\sqrt{\Gamma}}} & 0 & 0 & \dfrac{\sqrt{\Gamma - l_x\sqrt{\Gamma}}}{\sqrt{2\Gamma}} \end{bmatrix}^{\mathsf{T}}, & l_x < 0. \end{cases} \tag{34}$$

Finally, we can generalize the quaternion orientation of the global frame relative to the local frame as the multiplication of the two quaternions $\boldsymbol{q}_{\text{acc}}$ and $\boldsymbol{q}_{\text{mag}}$ as follows:

$$ {}^{L}_{G}\boldsymbol{q} = \boldsymbol{q}_{\text{acc}} \otimes \boldsymbol{q}_{\text{mag}}. \tag{35} $$

IV. Covariance Propagation

In this section, we analyze the propagation of the acceleration and magnetic field uncertainty throughout the algebraic quaternion formulation in Section III. We provide an estimation of its covariance matrix.

Given the standard deviation of the acceleration vector measured by the accelerometer and assuming that the three components are statistically independent between each other and normally distributed, we can easily recover the covariance matrix

$$ \boldsymbol{\Sigma}_{\text{acc}} = \begin{bmatrix} \sigma^2_{\text{acc}_x} & 0 & 0 \\ 0 & \sigma^2_{\text{acc}_y} & 0 \\ 0 & 0 & \sigma^2_{\text{acc}_z} \end{bmatrix} \tag{36} $$

where σ_{acc_x}, σ_{acc_y}, and σ_{acc_z} are, respectively, the standard deviations of the x, y, and z components of the local frame acceleration vector. In the formulation of Section III, the acceleration vector is normalized, and therefore the covariance matrix of (36) is no longer valid and the components are no longer independent. Let us assume that the total measured acceleration is always gravity with constant norm $\|\boldsymbol{a}\| = 9.81$ m/s^2. Under this assumption, we can still consider the three vector's components independent and, given their normal distribution, we can approximate the variance of each component as $\hat{\sigma}^2_{\text{acc}} = \sigma^2_{\text{acc}}/\|\boldsymbol{a}\|^2$. Hence, an approximation of the covariance matrix can be written as follows:

$$ \widehat{\boldsymbol{\Sigma}}_{\text{acc}} = \frac{1}{\|\boldsymbol{a}\|^2} \begin{bmatrix} \sigma^2_{\text{acc}_x} & 0 & 0 \\ 0 & \sigma^2_{\text{acc}_y} & 0 \\ 0 & 0 & \sigma^2_{\text{acc}_z} \end{bmatrix}. \tag{37} $$

Similarly, for the normalized magnetic field vector

$$ \widehat{\boldsymbol{\Sigma}}_{\text{mag}} = \frac{1}{\|\boldsymbol{m}\|^2} \begin{bmatrix} \sigma^2_{\text{mag}_x} & 0 & 0 \\ 0 & \sigma^2_{\text{mag}_y} & 0 \\ 0 & 0 & \sigma^2_{\text{mag}_z} \end{bmatrix} \tag{38} $$

where $\|\boldsymbol{m}\| = 0.52$ G is the current magnetic field norm in the New York area according to the World Magnetic Model [36].

The quaternion ${}^{L}_{G}\boldsymbol{q}$ is a function of both acceleration and magnetic field vector. For convenience, we consider these two vectors as a single input vector $\boldsymbol{u}$ as defined in the following:

$$ \boldsymbol{u} = [\, a_x \quad a_y \quad a_z \quad m_x \quad m_y \quad m_z \,]^{\mathsf{T}} \tag{39} $$

with diagonal covariance matrix

$$ \boldsymbol{\Sigma}_u = \begin{bmatrix} \widehat{\boldsymbol{\Sigma}}_{\text{acc}} & \mathbf{0}_{3\times3} \\ \mathbf{0}_{3\times3} & \widehat{\boldsymbol{\Sigma}}_{\text{mag}} \end{bmatrix}. \tag{40} $$

We want to model a Gaussian distribution of the quaternion ${}^{L}_{G}\boldsymbol{q}$ given the normally distributed input vector $\boldsymbol{u}$ and its uncertainty. However, since ${}^{L}_{G}\boldsymbol{q}$ is a nonlinear function of $\boldsymbol{u}$, we linearize it by approximation to a first-order Taylor expansion using its Jacobian matrix to propagate the uncertainty as in the linear case as follows:

$$ \boldsymbol{\Sigma}_q = \mathbf{J}\, \boldsymbol{\Sigma}_u\, \mathbf{J}^{\mathsf{T}} \tag{41} $$

where $\mathbf{J}$ is the 4×6 Jacobian matrix of the quaternion ${}^{L}_{G}\boldsymbol{q}$

$$ \mathbf{J} = \frac{\partial\left({}^{L}_{G}\boldsymbol{q}\right)}{\partial \boldsymbol{u}} = \begin{bmatrix} \frac{\partial q_0}{\partial a_x} & \frac{\partial q_0}{\partial a_y} & \frac{\partial q_0}{\partial a_z} & \frac{\partial q_0}{\partial m_x} & \frac{\partial q_0}{\partial m_y} & \frac{\partial q_0}{\partial m_z} \\ \frac{\partial q_1}{\partial a_x} & \frac{\partial q_1}{\partial a_y} & \frac{\partial q_1}{\partial a_z} & \frac{\partial q_1}{\partial m_x} & \frac{\partial q_1}{\partial m_y} & \frac{\partial q_1}{\partial m_z} \\ \frac{\partial q_2}{\partial a_x} & \frac{\partial q_2}{\partial a_y} & \frac{\partial q_2}{\partial a_z} & \frac{\partial q_2}{\partial m_x} & \frac{\partial q_2}{\partial m_y} & \frac{\partial q_2}{\partial m_z} \\ \frac{\partial q_3}{\partial a_x} & \frac{\partial q_3}{\partial a_y} & \frac{\partial q_3}{\partial a_z} & \frac{\partial q_3}{\partial m_x} & \frac{\partial q_3}{\partial m_y} & \frac{\partial q_3}{\partial m_z} \end{bmatrix}. \tag{42} $$

In practice, we do not compute the Jacobian matrix as in (42) because the quaternion ${}^{L}_{G}\boldsymbol{q}$, directly expressed as a function of $\boldsymbol{a}$ and $\boldsymbol{m}$, has a long form and its use in the partial derivative computation would result in a complicated matrix. Instead, we consider the quaternion measurement as a composition of functions, and then we apply the chain rule to find the final Jacobian matrix.

We first consider the quaternion ${}^{L}_{G}\boldsymbol{q}$ as a function of $\boldsymbol{q}_{\text{acc}}$ and $\boldsymbol{q}_{\text{mag}}$. These two quaternions are functions, respectively, of $\boldsymbol{a}$ and $\boldsymbol{l}$, where $\boldsymbol{l}$ is the function of $\boldsymbol{u}$. For clarity, we define the following two vector functions:

$$ \boldsymbol{f}_1(\boldsymbol{a}, \boldsymbol{l}) = [\, \boldsymbol{q}_{\text{acc}} \quad \boldsymbol{q}_{\text{mag}} \,], \quad \boldsymbol{f}_2(\boldsymbol{u}) = [\, \boldsymbol{a} \quad \boldsymbol{l} \,] \tag{43} $$

and more simply describe the explicit and implicit dependencies of ${}^{L}_{G}\boldsymbol{q}$

$$ {}^{L}_{G}\boldsymbol{q} \equiv {}^{L}_{G}\boldsymbol{q}(\boldsymbol{f_1}(\boldsymbol{f_2}(\boldsymbol{u}))). \tag{44} $$

It is now clear that the Jacobian matrix of (42) can be calculated using the following chain rule:

$$ \mathbf{J} = \frac{\partial\left({}^{L}_{G}\boldsymbol{q}\right)}{\partial \boldsymbol{f}_1} \frac{\partial \boldsymbol{f}_1}{\partial \boldsymbol{f}_2} \frac{\partial \boldsymbol{f}_2}{\partial \boldsymbol{u}}. \tag{45} $$

The actual values of the Jacobian matrices are reported in the Appendix.

Fig. 1 shows the components of the quaternion orientation during a simulated rotation with constant angular velocities of 0.1 rad/s around the x-axis, -0.2 rad/s around the y-axis, and 0.1 rad/s around the z-axis. We selected the noise of the acceleration and magnetic field vectors to have standard deviations of $\sigma_a = 0.001$ m/s^2 and $\sigma_m = 0.001$ G for all the three axes. Such angular velocity and noise standard deviation values were chosen only for visualization purposes and any other value would provide correct results as well. To obtain the result in Fig. 1, we first assume that the acceleration is a Gaussian random vector with mean $\boldsymbol{\mu}_a = \overline{\boldsymbol{a}}$ and covariance matrix $\boldsymbol{\Sigma}_{\text{acc}}$ as summarized in the following:

$$ {}^{L}\boldsymbol{a} = \mathcal{N}\left(\boldsymbol{\mu}_a = \overline{\boldsymbol{a}},\ \boldsymbol{\Sigma}_{\text{acc}}\right) \tag{46} $$

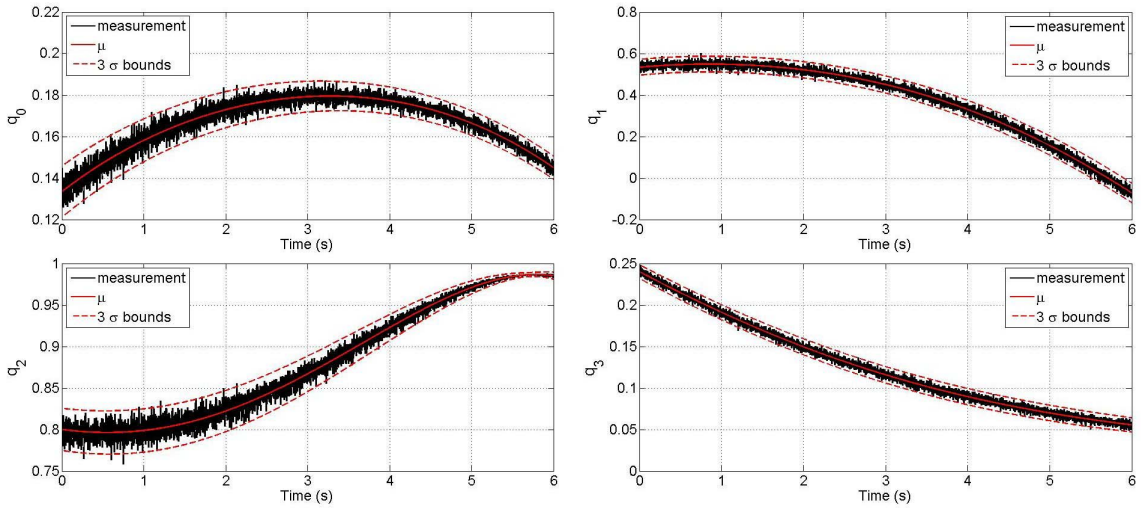

Fig. 1. Quaternions components, mean and measurement, and the 3σ boundaries during a simulated rigid body rotation.

where $\overline{\boldsymbol{a}}$ is the noise-free acceleration vector and $\boldsymbol{\Sigma}_{\text{acc}}$ characterizes the amount of noise we added in $\overline{\boldsymbol{a}}$ to obtain ${}^{L}\boldsymbol{a}$. Similarly, for the magnetic field vector

$$ {}^{L}\boldsymbol{m} = \mathcal{N}\big(\boldsymbol{\mu}_m = \overline{\boldsymbol{m}},\ \boldsymbol{\Sigma}_{\text{mag}}\big). \tag{47} $$

As we saw in the previous section, the quaternion ${}^{L}_{G}\boldsymbol{q}$, computed using algebraic quaternion algorithm (AQUA), is a function of ${}^{L}\boldsymbol{a}$ and ${}^{L}\boldsymbol{m}$ through (24), (34), and (35). Thus, we can write ${}^{L}_{G}\boldsymbol{q} = \boldsymbol{f}({}^{L}\boldsymbol{a}, {}^{L}\boldsymbol{m})$. This value is what we call measurement. We approximate it as a normally distributed random vector assuming that its mean directly derives from the AQUA by processing the noise-free acceleration and magnetic field vectors, while its uncertainty comes from the propagation of the acceleration and magnetic field covariances (41) as summarized in the following:

$$ {}^{L}_{G}\boldsymbol{q} \approx \mathcal{N}\big(\boldsymbol{\mu} = \boldsymbol{f}(\overline{\boldsymbol{a}}, \overline{\boldsymbol{m}}),\ \boldsymbol{\Sigma}_q = \boldsymbol{\eta}\big(\boldsymbol{\Sigma}_{\text{acc}}, \boldsymbol{\Sigma}_{\text{mag}}\big)\big). \tag{48} $$

Finally, we plot the components of the quaternion measurement $[{}^{L}_{G}\boldsymbol{q} = \boldsymbol{f}({}^{L}\boldsymbol{a}, {}^{L}\boldsymbol{m})]$, their mean, and the 3σ boundaries, acknowledging that the standard deviations of the quaternion components are the square root of the diagonal terms of the covariance matrix $\boldsymbol{\Sigma}_q$. Using this procedure, we demonstrate that the calculated boundaries properly enclose the quaternion measurement affected by the noise coming from the sensors readings, propagated through the process explained in Section III.

V. Kalman Filter Design

In this section, we present the design of a novel quaternion-based Kalman filter with a four-state vector (the quaternion components) and linear process and measurements models. The novel approach employs our external algorithm (AQUA) to find the quaternion orientation of the rigid body as an algebraic solution of a system using earth field data from a MARG sensor. The computed quaternion is taken as measurement for the Kalman filter to correct the predicted state obtained by processing the readings provided by the angular rate sensor. Using this method, all the output equations are linear, simplifying the design of the filter. Unlike other linear quaternion-based filters previously proposed [9], [31], we do not find the quaternion correction as output of an optimization algorithm, but as an algebraic solution that ensures fast convergence rate of the orientation estimation. The block diagram of the proposed filter is shown in Fig. 2.

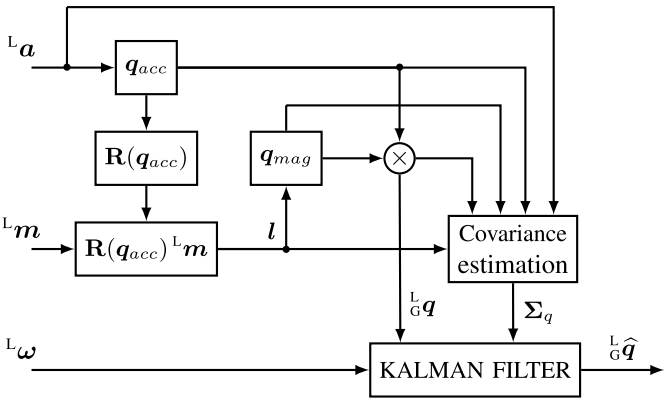

Fig. 2. Block diagram of the proposed quaternion-based Kalman filter for MARG sensors.

The orientation of a rigid body in space is determined by the representation of the coordinate frame attached to the body (the local frame L) with respect to the absolute coordinate system (the global frame G). To simplify the calculations in the following sections, we will refer to the orientation of the global frame expressed with respect to the local frame. The state vector of the proposed filter is composed of the four quaternion components as follows:

$$ \boldsymbol{x}_{k+1} = {}^{L}_{G}\boldsymbol{q} = [q_0 \quad q_1 \quad q_2 \quad q_3]^{\mathsf{T}}. \tag{49} $$

In this paper, we do not estimate the biases of the input measurement vectors; however, a typical state augmentation technique could be adopted to address this matter.

The initial quaternion estimate is given by the output of the AQUA allowing a fast filter initialization in any starting configuration.

A. Process Model

In the prediction step, the angular velocity vector, measured by the triaxis gyroscope, is used to compute the first estimation of the orientation in quaternion form. It is well known that the rigid body angular motion obeys a vector differential equation describing the rate of change of the orientation as quaternion derivative [26]

$$ {}^{L}_{G}\dot{\boldsymbol{q}}_{\omega,t} = -\frac{1}{2}{}^{L}\boldsymbol{\omega}_{q,t} \otimes {}^{L}_{G}\boldsymbol{q}_{t}. \tag{50} $$

The above equation can be rewritten in matrix form as shown in

$$ {}^{L}_{G}\dot{\boldsymbol{q}}_{\omega,t} = \boldsymbol{\Omega}({}^{L}\boldsymbol{\omega}){}^{L}_{G}\boldsymbol{q}_{t} \tag{51} $$

where

$$ \boldsymbol{\Omega}({}^{L}\boldsymbol{\omega}_{t}) = \begin{bmatrix} 0 & {}^{L}\boldsymbol{\omega}_{t}{}^{\mathsf{T}} \\ -{}^{L}\boldsymbol{\omega}_{t} & -[{}^{L}\boldsymbol{\omega}_{t}\times] \end{bmatrix} \tag{52} $$

and, regardless of the time dependence, the term $[{}^{L}\boldsymbol{\omega}\times]$ denotes the cross-product matrix that is associated with ${}^{L}\boldsymbol{\omega}$ and is equal to

$$ [{}^{L}\boldsymbol{\omega}\times] = \begin{bmatrix} 0 & -\omega_z & \omega_y \\ \omega_z & 0 & -\omega_x \\ -\omega_y & \omega_x & 0 \end{bmatrix}. \tag{53} $$

The orientation of the global frame relative to the local frame at time t can be computed by numerically integrating the quaternion derivative using the sampling period Δt. The discrete state transition vector equation, which characterizes the process model, is derived from (51) and is presented in the following:

$$ \boldsymbol{x}_{k+1} = \boldsymbol{\Phi}({}^{L}\boldsymbol{\omega}, \Delta t)\boldsymbol{x}_{k} + \boldsymbol{w}_{k} \tag{54} $$

where the state transition matrix is computed using a zeroth-order integration

$$ \boldsymbol{\Phi}({}^{L}\boldsymbol{\omega}, \Delta t) \approx \left[\mathbf{I}_{4\times4} + \frac{1}{2}\boldsymbol{\Omega}_{\boldsymbol{k}}({}^{L}\boldsymbol{\omega})\Delta t\right] \tag{55} $$

and

$$ \boldsymbol{w}_{k} = -\frac{\Delta t}{2}\boldsymbol{\Xi}_{k}\boldsymbol{v}_{g_k} = -\frac{\Delta t}{2}\begin{bmatrix} q_1 & q_2 & q_3 \\ -q_0 & -q_3 & -q_2 \\ q_2 & -q_0 & -q_1 \\ -q_2 & q_1 & -q_0 \end{bmatrix}\boldsymbol{v}_{g_k} \tag{56} $$

where $\boldsymbol{v}_{g_k}$ is the white Gaussian measurement noise affecting the gyroscope readings, with covariance matrix $\boldsymbol{\Sigma}_{\mathbf{g}} = \sigma_g^2\,\mathbf{I}_{3\times3}$. Finally, the process noise covariance matrix $\mathbf{Q_k}$ is equal to

$$ \mathbf{Q_k} = \left(-\frac{\Delta t}{2}\right)^{2}\boldsymbol{\Xi}_{k}\boldsymbol{\Sigma}_{\mathbf{g}}\boldsymbol{\Xi}_{k}{}^{\mathsf{T}}. \tag{57} $$

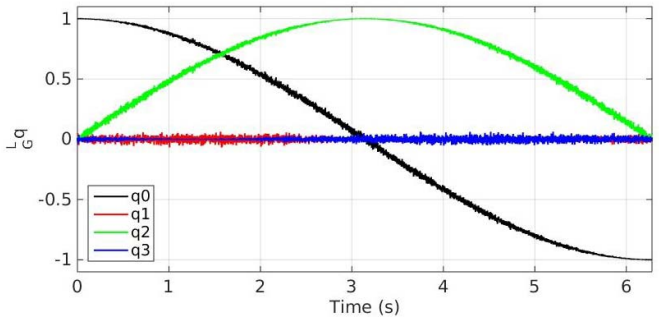

Fig. 3. Final quaternion orientation of the global frame with respect to the local frame in a 180° rotation about the y-axis, found as quaternion multiplication between $\boldsymbol{q}_{\text{acc}}$ and $\boldsymbol{q}_{\text{mag}}$. The quaternion does not incur in singularities, and as a result of the continuity test, it is continuous throughout the rotation.

B. Measurement Model

The measurement update step applies the quaternion obtained from the AQUA analyzed in Section III. We can then write

$$ z_{k+1} = {}^{L}_{G}\boldsymbol{q}_{k+1} + \boldsymbol{w}_{z_{k+1}} \tag{58} $$

where $\boldsymbol{w}_{z_{k+1}}$ is the measurement noise approximated as a white Gaussian noise obtained from the propagation of the acceleration and magnetic field measurement noises via the process of Section III. Finally, the measurement noise covariance matrix $\mathbf{R}_{k+1}$ will have the value previously found in the covariance propagation part discussed in Section IV. Thus, in terms of the measurement process, we can write

$$ \mathbf{R}_{k+1} = \boldsymbol{\Sigma}_{q_{k+1}} \tag{59} $$

where $\boldsymbol{\Sigma}_{q_{k+1}}$ is the covariance matrix computed in (41). In this new approach, both process model and measurement model are linear, and therefore the implementation of the proposed filter uses the regular Kalman filter's equations [37]. The estimated state variables, which are the four quaternion components, are related by the unit-norm constraint that is not preserved by the Kalman filter equations. In order to preserve the quaternion unit-norm property, the filter developed in this paper adopts a final normalization step to normalize the estimate after the measurement update stage.

The quaternion representing the orientation of the global frame with respect to the local frame, calculated as per (35), may have some discontinuities because the orientation can be represented using two alternative rotation paths. When using quaternions to represent the orientation, the alternative rotation path is given by switching the sign of all the quaternion components. This feature does not pose any problem in the orientation representation. However, when the algebraic quaternion is adopted in the correction step of an additive Kalman filter, its value must be consistent with the current state. To resolve this issue, we check the angular difference between the two quantities, in each updating step, by calculating their dot product [38]. If the dot product is positive, we keep the current quaternion measurement; otherwise, we use the negative quaternion, which represents the alternative rotation path. Fig. 3 shows the final quaternion in a simulated 180° rotation

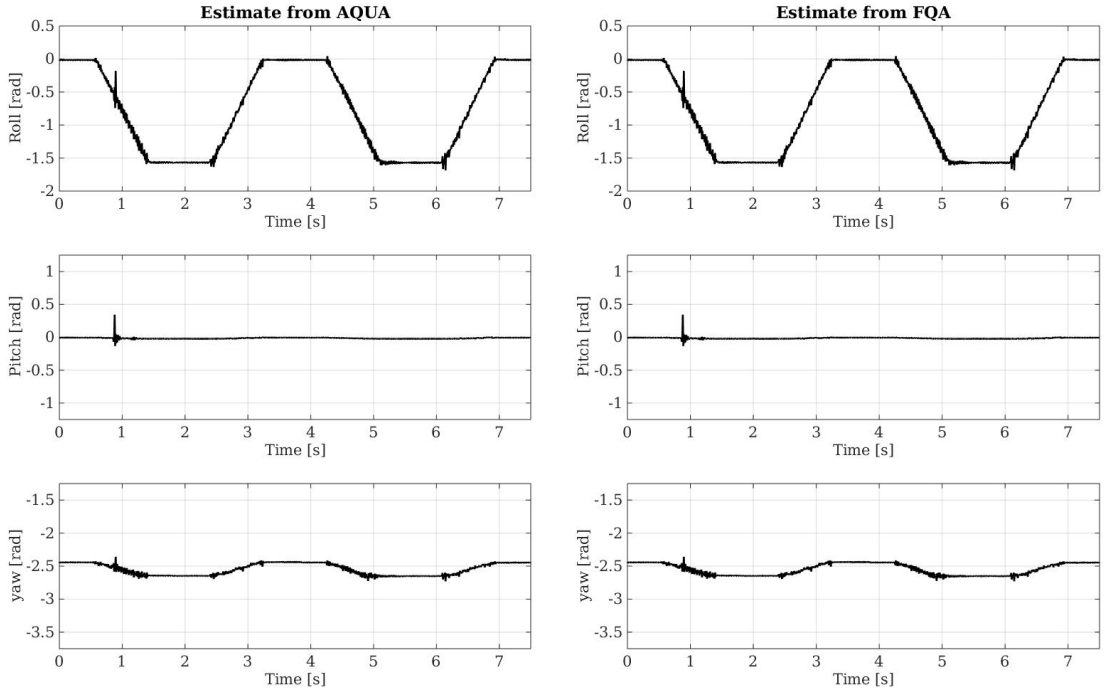

Fig. 4. Orientation estimate produced by AQUA and FQA with a periodic 90° rotation about the x-axis using accelerometer and magnetometer data.

around the y-axis, after being subjected to the test explained above using the quaternion found from the angular velocity, by numerical integration of (50), as reference. The quaternion does not incur in the singularity state, and as a result of the continuity test, it is continuous throughout the rotation.

VI. Results and Discussion

In this section, we evaluate the performances of the proposed AQUA compared against the FQA [34] using simulated data and show some results with real data from a PhidgetSpatial 3/3/3 MARG sensor [39].

Furthermore, we analyze the behavior of the proposed Kalman filter under different conditions and compare it against the extended Kalman filter proposed in [24] and against the filter in [17]. The EKF presented in [24] has the structure of a typical quaternion-based EKF [9], [10], [23] with the state composed of the unit quaternion components and augmented with magnetic distortion vector, modeled as a Gauss–Markov process, to reduce the heading drift in magnetically nonhomogeneous environments. The filter proposed in [17] is a constant gain filter that corrects the drift of the gyroscope integration by means of a gradient-descent algorithm employed to find a quaternion orientation from acceleration and magnetic field measurements. Such an approach offers magnetic distortion compensation thanks to the construction of the quaternion correction in which magnetic disturbances affect only the heading component.

A. Algebraic Quaternion Algorithm Results

To test the effectiveness of our algorithm, we used MATLAB to simulate three consecutive constant velocity rotations of 360° about each axis with the respective acceleration and magnetic field data affected by Gaussian noise. We implemented both algorithms AQUA and FQA to find the quaternion orientation throughout the rotations, and we compared the results. We found that the two algorithms provide the quaternions with the same accuracy; however, AQUA is 65% computationally more efficient than FQA. This result is justified by the fact that AQUA performs only one quaternion multiplication against the three of FQA. Furthermore, the first method solves the singularity using a switching technique between two different formulations of the quaternion, without adding any extra computational burden, whereas FQA needs to rotate both acceleration and magnetic field vectors by an offset angle, which will be corrected in the final calculation of the quaternion orientation, by including an extra quaternion multiplication. Note that another advantage of AQUA over FQA is that the former does not need *a priori* knowledge of the direction of the earth's magnetic field (${}^G\boldsymbol{h}$), whereas in the latter, this knowledge is necessary to calculate the azimuth quaternion.

To show the results using real data, we proposed an experiment similar to the one executed in [34] to compare the FQA against the QUEST algorithm. Controlled rotations of the MARG sensor were performed by attaching the sensor to a servomotor. The sensor was placed over the axis of rotation of the servomotor in order to reduce any nongravitational acceleration that might occur during the motion in case of misalignment. We used a Hitec HS 422 servomotor, with a resolution of 0.35°, connected to a microcontroller programmed to alternately rotate the servomotor with a constant rate of 90°/s by ±90° and stop for 1 s at angles 0° and ±90°. Fig. 4 shows the orientation expressed in Euler angles as a result of rotations about the x-axis using raw accelerometer

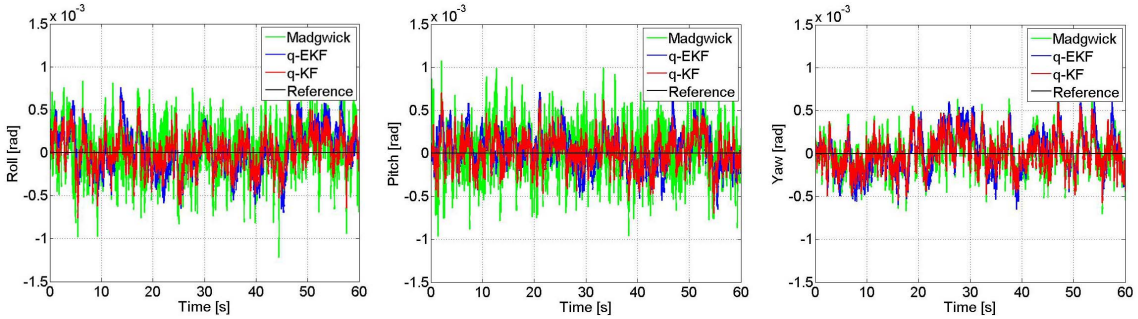

Fig. 5. Euler representation of the orientation produced by the three filters, using simulated data in static condition.

and magnetometer data. Similar results were obtained for rotations about the other axes. Note that the yaw motion seen in the yaw subplot is due to the magnetic field generated by the motor. Fig. 4 shows that the two methods have a similar behavior and performances as already proved with simulated data.

B. Kalman Filter

In this section, we provide the results regarding the proposed Kalman filter and comparisons against the extended Kalman filter and the Madgwick filter. At first, we evaluate the filters' performances by quantifying the static and dynamic root-mean-square (rms) errors of the outputs of the two filters using simulated data to provide ground truth. Afterward, we analyzed the behavior of the two approaches using real data from a PhidgetSpatial 3/3/3 [39] sensor during fast rotations and in a magnetically disturbed environment.

1) Simulation: In the simulated experiments, we quantify the rms error of the orientation output of the two filters expressed as Euler angles. We simulated angular velocity, acceleration, and magnetic field data as affected by white Gaussian noise with standard deviations of $\sigma_g = 0.004$ rad/s, $\sigma_a = 0.014$ m/s^2, and $\sigma_m = 0.001$ G, respectively, where for each vector, the standard deviations are the same for all the axes. The selected standard deviations are the ones we empirically found to be the standard deviations of the noise that affect the readings of the MARG sensor we used for real data experiment as explained in the next section. In the case of the Madgwick filter, we selected the gain that minimizes the rms error. Such a value was found to be $\beta = 0.0087$; it is very low because no bias was included in the simulated angular velocity measurements. Fig. 5 shows the roll, pitch, and yaw angles' output of the algorithms during the first simulated experiment, which is performed to evaluate the static rms error on a total time of 1 min. The second experiment simulates three simultaneous rotations about the sensor frame's axes, for a total duration of 1 min, with the following constant angular velocities: $\omega_x = \omega_y = \omega_z = 0.1$ rad/s and with an additional linear acceleration of 0.1 m/s^2 along all the axes. The results of both simulations are summarized in Table I where the values of static and dynamic rms errors are listed for all the algorithms, showing better results of the proposed one in every scenario.

2) Fast Rotations: In this experiment, we tested the performances of the three algorithms during fast rotations using real data, by manually rotating the sensor around the x and y axes. We used the PhidgetSpatial 3/3/3 sensor [39]. It provides acceleration, angular rate, and magnetic field strength measurements in three axes. We measured the standard deviation of each quantity provided by the device, over a total amount of 10^4 readings, obtaining the following values for the angular velocity, acceleration, and magnetic field vector, respectively: $\sigma_{g_x} = \sigma_{g_y} = \sigma_{g_z} = 0.004$ rad/s, $\sigma_{a_x} = \sigma_{a_y} = \sigma_{a_z} = 0.014$ m/s^2, and $\sigma_{m_x} = \sigma_{m_y} = \sigma_{m_z} = 0.001$ G. These values are then input into the Kalman filter and extended Kalman filter to obtain the noise process and measurement covariance matrices. The gain parameter of the Madgwick filter adopted in the experiments performed using the Phidgets sensor was selected as the value that ensures the rate of divergence of the quaternion from gyro integration to be equal to the rate of convergence of the correction term as discussed in [17]. For the application of the algorithm with the sensor we employed, such a gain value is $\beta = 0.093$.

The experiment is meant to show the ability of each algorithm to track rapid attitude variations without giving any information about the accuracy of the algorithms. We first executed two manual 360° rotations of the sensor around its x-axis; then, we repeated the same maneuvers around the y-axis. No rotation around the z-axis was performed because, unlike the other filters, the current implementation of our KF works only for MARG sensors (with magnetic field data). Therefore, since the experiment was performed in a magnetically nonhomogeneous environment, the output of rotations around the z-axis would be affected by magnetic disturbances providing unreliable results.

The first rotation was executed at a slower angle rate to allow all the filters to successfully track the angle throughout the rotation. Afterward, during the second faster rotation, only

TABLE I

STATIC AND DYNAMIC rms ERRORS OF THE PROPOSED QUATERNION-BASED KF, THE QUATERNION-BASED EKF, AND THE CONSTANT GAIN FILTER BY MADGWICK *et al.* [17]

RMS error	**q-KF** [rad]	**q-EKF** [rad]	**Madgwick**
roll static	2.10×10^{-4}	2.65×10^{-4}	2.834×10^{-4}
roll dynamic	7.43×10^{-3}	9.41×10^{-3}	1.25×10^{-2}
pitch static	2.04×10^{-4}	2.15×10^{-4}	2.89×10^{-4}
pitch dynamic	8.22×10^{-3}	1.03×10^{-2}	1.11×10^{-2}
yaw static	1.92×10^{-4}	2.43×10^{-4}	2.13×10^{-4}
yaw dynamic	8.51×10^{-3}	1.24×10^{-2}	1.41×10^{-3}

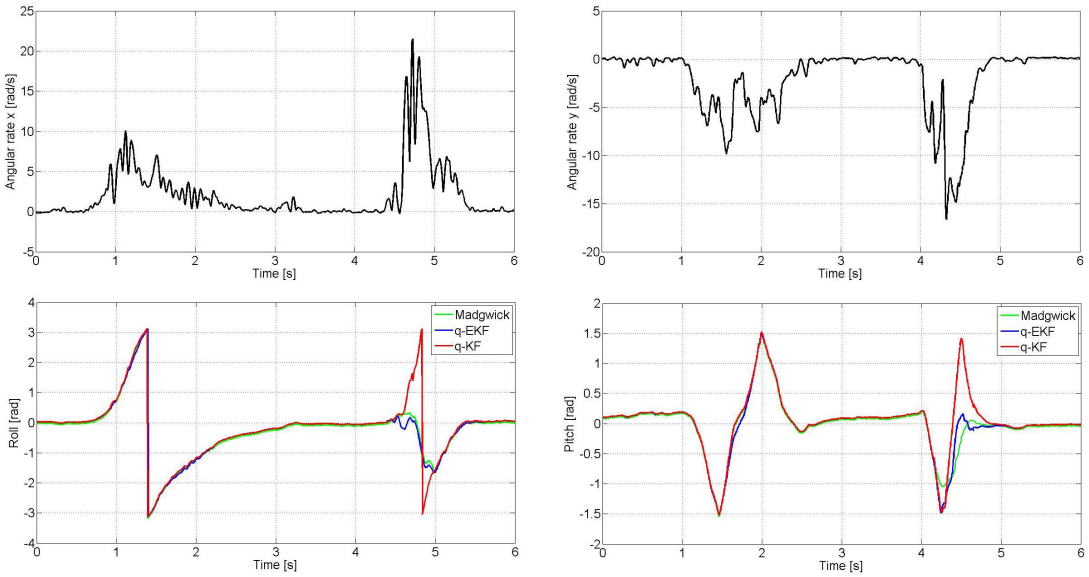

Fig. 6. Two complete 360° rotations about the x-axis (left) and the y-axis (right). Top: angular velocities during the rotations. Bottom: roll and pitch angles' output of the three filters. The first rotation is executed at a slower rate to allow all the filters to provide the correct orientation, while the second faster rotation is correctly followed only by the proposed Kalman filter.

the proposed Kalman filter was able to continuously track the angle's variation as shown in Fig. 6. Fig. 6 (top) shows the value of the angular velocities during all the experiments, and Fig. 6 (bottom) shows the resulting roll and pitch angles' output of the two algorithms. Because we performed the rotations manually, we could not maintain a constant angular velocity during the rotations, but we can provide the average values that are $\omega_{x_1} = 2.22$ and $\omega_{x_2} = 6.68$ rad/s for the two complete rotations around the sensor's x-axis and $\omega_{y_1} = -3.81$ and $\omega_{y_2} = -8.57$ rad/s for the two complete rotations around the y-axis. By performing the rotations manually, we cannot replicate the experiment with the same rotational speed and provide a rigorous statistical analysis. However, we repeated similar trials for five times on each axis trying to maintain the angular velocity with an average value between 6 and 9 rad/s always yielding the same result.

The ability of our algorithm to track rapid changes in the attitude is given by the novel formulation of the quaternion measurement (explained in Section III) that is found as an algebraic solution in a single fast step, instead of the output of an optimization algorithm.

3) Magnetic Disturbances: In the third experiment, we used the sensor previously described, with the measured standard deviations listed in the previous section, and the same gain value was adopted for the Madgwick filter. We held the sensor steady on the horizontal plane (zero roll and pitch) while reading the output of the filters. We induced magnetic disturbances by approaching a big magnet to the sensor following a horizontal path along the sensor's x-axis and repeated this action twice. For the first time, we applied the magnetic disturbance for about 4 s and then we removed it, whereas for the second time, we retained the disturbance until the end of the experiment.

Fig. 7 shows the results of the experiment. Fig. 7(a) shows the norm of the magnetic field vector, allowing the reader to have a better understanding of the experiment by visualizing the norm variations, which evince the time at which the disturbance is either applied or removed. Fig. 7 also shows

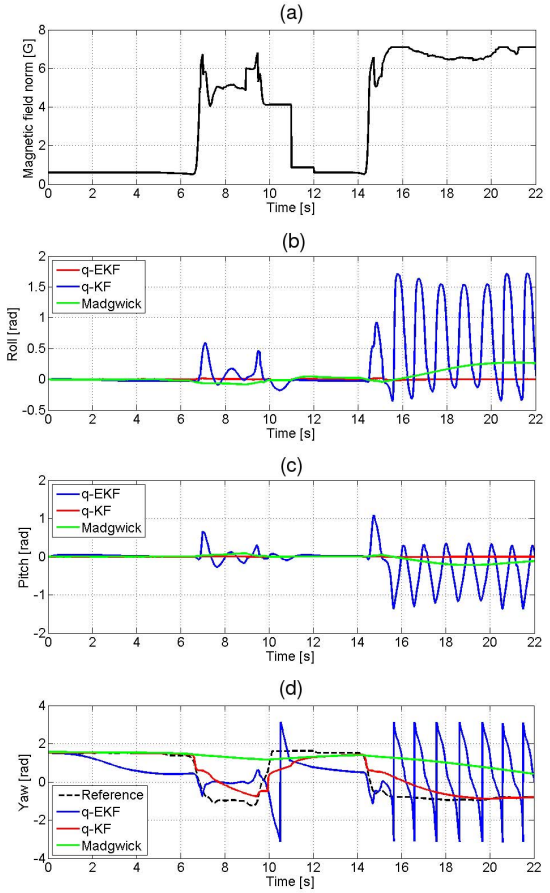

Fig. 7. Orientation estimation in a magnetically disturbed environment. (a) Norm of the magnetic field measured by the sensor that is abruptly changed when the magnet is approached and departed. (b)–(d) Behavior of the filters under such a condition, through the visualization of the orientation in Euler angles.

that the roll and pitch angles from our Kalman filter are immune to magnetic disturbances, whereas the roll and pitch from the EKF are affected by the magnetic disturbances when we approach the magnet to the sensor, converging back to the right value when the disturbance is removed. When we induce the disturbance the second time, the roll and pitch of the EKF oscillate indefinitely because of the presence of the high magnetic field of the magnet. The behavior of the EKF is a consequence of the coupled nature of the acceleration and magnetic field correction. The roll and pitch from the Madgwick filter are affected by variable magnetic fluxes. Indeed, the angles experience a relevant error when we approach and remove the magnet from the sensor, slowly converging back to the right value when the disturbance is maintained constant.

In a magnetically homogeneous environment, the global magnetic field vector ${}^{G}\boldsymbol{h}$ is supposed to be constant; therefore, under this assumption, the EKF uses the value of the global magnetic field perceived in the local area as predefined reference of the filter. However, when this reference is altered by local disturbances, the EKF will respond with an unstable behavior where even the yaw angle does not simply follow the reference, but it continues to drift as demonstrated in Fig. 7(d). In Fig. 7(d), we show the yaw angles' output of the algorithms during the same experiment, compared against the reference yaw angle extracted from the magnetic field vector previously projected onto the horizontal plane. This yaw reference does not have to be confused with the ground truth, as in this experiment, the sensor is kept steady and the true yaw is constant and equal to the value that the yaw reference assumes at the beginning of the experiment. Instead, the yaw reference is the angle between the current direction of the sensor's x-axis and the direction of the reference magnetic field vector as perceived by the magnetometer under the influence of the magnetic disturbances. Unlike the EKF, our KF does not need the predefined knowledge of the reference direction; hence, the variation of the magnetic field will be seen as a simple change of the heading that will be tracked by the yaw output as shown in Fig. 7(d). The yaw output of the Madgwick filter has a similar behavior to the yaw of our Kalman filter but with slower convergence rate, which, in this case, leads to better results. However, when the variation of the magnetic field is not caused by disturbances, but it comes from actual heading variations, the slower convergence reduces the tracking performances of the filter.

Ultimately, we analyzed the computational time of the three methods. We profiled a reasonably optimized C++ implementation of the algorithms running on an Intel core I7 3.6-GHz processor. Note that unlike the previous experiments, where the complete state vector of the EKF was adopted, in this analysis for a fair runtime comparison, we used an implementation of the EKF that has only the four quaternion components as the state vector (without bias and magnetic disturbance estimation). The results of the average execution time of a prediction–correction update cycle are listed in Table II. The results demonstrate that the constant gain filter is clearly the faster approach due to the simpler estimation approach, which avoids any statistical analysis.

TABLE II
COMPUTATIONAL TIME OF THE ESTIMATION ALGORITHMS

Algorithm	Average time(μs)	Standard deviation(μs)
Madgwick	1.2839	0.7101
q-KF	3.9605	0.1972
q-EKF	7.0408	0.2342

Nonetheless, the proposed KF is faster than the EKF and shows a good tradeoff between computational load and accuracy, making it more suitable for small embedded processors.

VII. CONCLUSION

In this paper, we presented a method to find the quaternion orientation of the global frame with respect to the local frame as an algebraic solution to Whaba's problem through the observations of gravity and magnetic field from inertial/magnetic sensors. The subdivision of the quaternion in two parts makes the roll and pitch components immune to magnetic distortions. We compared our method against the FQA. Although the level of accuracy of both methods is the same, our method is about 65% computationally more efficient, and unlike the FQA, the procedure we adopted to find the heading component of the orientation eliminates the need for a direction magnetic field to be predefined.

We provided an estimation of the covariance of the quaternion output of the novel algorithm, assuming its Gaussian distribution. The covariance estimation allows the users to adopt the orientation estimation in all those applications where an evaluation of its uncertainty is required. A typical application where an input measurement is requested along with the estimate of its uncertainty is the Kalman filter. To prove the effectiveness of our method used in conjunction with other sources of orientation in a sensor fusion algorithm, we implemented a linear quaternion-based Kalman filter. The current implementation of the filter does not include the estimation of the sensors' biases and does not address the problem of the external acceleration. However, common techniques, such as state augmentation (for bias estimation) and adaptive covariance matrix (to reduce the effect of the external acceleration), can be adapted to the proposed filter.

The Kalman filter employs the output of the AQUA as the input measurement of the update step in a two-layer architecture. This approach makes the measurement model linear, reducing the complexity of the filter. We tested the performances of the proposed KF in different working conditions and compared them against an AEKF and a constant gain filter that offer magnetic compensation. The linear KF has slightly better static and dynamic rms errors that we evaluated in simulated experiments. Furthermore, we demonstrated the higher convergence rate of the proposed filter, using real IMU data, performing fast rotations, which the other approaches were not able to follow. Such results are possible thanks to the input measurement that is already in quaternion form as output of the fast algebraic algorithm. Moreover, unlike the other filters, the roll and pitch

components of the orientation produced by the KF are immune to magnetic disturbances.

APPENDIX

In this section, we provide the Jacobian matrices resulting from the derivation described in Section IV. We have two different sets of Jacobian matrices, depending on the sign of the acceleration vector z-component, because of the switching configuration of $\boldsymbol{q}_{\text{acc}}$ in (24) used to avoid the singularity. In this manner, we also prevent from having an infinite covariance matrix. The matrices are listed in the following, where for $a_z \geq 0$:

$$\frac{\partial \left({}^{L}_{G}\boldsymbol{q}\right)}{\partial \boldsymbol{f}_1} = \begin{bmatrix} q_{0_m} & 0 & 0 & -q_{3_m} & q_{0_a} & -q_{1_a} & q_{2_a} & 0 \\ 0 & q_{0_m} & q_{3_m} & 0 & q_{1_a} & q_{0_a} & 0 & q_{2_a} \\ 0 & -q_{3_m} & q_{0_m} & 0 & q_{2_a} & 0 & q_{0_a} & -q_{1_a} \\ q_{3_m} & 0 & 0 & q_{0_m} & 0 & -q_{2_a} & q_{1_a} & q_{0_a} \end{bmatrix} \tag{60}$$

$$\frac{\partial \boldsymbol{f}_1}{\partial \boldsymbol{f}_2} = \frac{1}{2\sqrt{2}} \begin{bmatrix} 0 & 0 & \frac{1}{\kappa} & 0 & 0 & 0 \\ 0 & -\frac{2}{\kappa} & \frac{a_y}{\kappa^3} & 0 & 0 & 0 \\ \frac{2}{\kappa} & 0 & -\frac{a_x}{\kappa^3} & 0 & 0 & 0 \\ 0 & 0 & 0 & 0 & 0 & 0 \\ 0 & 0 & 0 & \frac{l_y^2}{\beta_1 \gamma} & \frac{l_x l_y}{\beta_1 \gamma} & 0 \\ 0 & 0 & 0 & 0 & 0 & 0 \\ 0 & 0 & 0 & 0 & 0 & 0 \\ 0 & 0 & 0 & -\frac{l_y \beta_1}{\gamma^{\frac{3}{2}}} & \frac{l_x \beta_1}{\gamma^{\frac{3}{2}}} & 0 \end{bmatrix} \quad l_x > 0 \tag{61}$$

$$\frac{\partial \boldsymbol{f}_1}{\partial \boldsymbol{f}_2} = \frac{1}{2\sqrt{2}} \begin{bmatrix} 0 & 0 & \frac{1}{\kappa} & 0 & 0 & 0 \\ 0 & -\frac{2}{\kappa} & \frac{a_y}{\kappa^3} & 0 & 0 & 0 \\ \frac{2}{\kappa} & 0 & -\frac{a_x}{\kappa^3} & 0 & 0 & 0 \\ 0 & 0 & 0 & 0 & 0 & 0 \\ 0 & 0 & 0 & \frac{l_y \beta_2}{\gamma^{\frac{3}{2}}} & \frac{l_x \beta_2}{\gamma^{\frac{3}{2}}} & 0 \\ 0 & 0 & 0 & 0 & 0 & 0 \\ 0 & 0 & 0 & 0 & 0 & 0 \\ 0 & 0 & 0 & -\frac{l_y^2}{\beta_2 \gamma} & \frac{l_x l_y}{\beta_2 \gamma} & 0 \end{bmatrix} \quad l_x < 0 \tag{62}$$

and $(\partial \boldsymbol{f}_2 / \partial \boldsymbol{u})$ as per (63), as shown at the bottom of this page, with

$$\kappa = \sqrt{1 + a_z}; \quad \gamma = l_x^2 + l_y^2$$

and

$$\beta_1 = \sqrt{\gamma + lx\sqrt{\gamma}}; \quad \beta_2 = \sqrt{\gamma - lx\sqrt{\gamma}}$$

and, for $a_z < 0$

$$\frac{\partial \left({}^{L}_{G}\boldsymbol{q}\right)}{\partial \boldsymbol{f}_1} = \begin{bmatrix} q_{0_m} & 0 & 0 & -q_{3_m} & q_{0_a} & -q_{1_a} & 0 & -q_{3_a} \\ 0 & q_{0_m} & q_{3_m} & 0 & q_{1_a} & q_{0_a} & -q_{3_a} & 0 \\ 0 & -q_{3_m} & q_{0_m} & 0 & 0 & q_{3_{\text{acc}}} & q_{0_a} & -q_{1_a} \\ q_{3_m} & 0 & 0 & q_{0_m} & q_{3_a} & 0 & q_{1_a} & q_{0_a} \end{bmatrix} \tag{64}$$

$$\frac{\partial \boldsymbol{f}_1}{\partial \boldsymbol{f}_2} = \frac{1}{2\sqrt{2}} \begin{bmatrix} 0 & -\frac{2}{\kappa} & -\frac{a_y}{\kappa^3} & 0 & 0 & 0 \\ 0 & 0 & -\frac{1}{\kappa} & 0 & 0 & 0 \\ 0 & 0 & 0 & 0 & 0 & 0 \\ \frac{2}{\kappa} & 0 & \frac{a_x}{\kappa^3} & 0 & 0 & 0 \\ 0 & 0 & 0 & \frac{l_y^2}{\beta_1 \gamma} & -\frac{l_x l_y}{\beta_1 \gamma} & 0 \\ 0 & 0 & 0 & 0 & 0 & 0 \\ 0 & 0 & 0 & 0 & 0 & 0 \\ 0 & 0 & 0 & -\frac{l_y \beta_1}{\gamma^{\frac{3}{2}}} & \frac{l_x \beta_1}{\gamma^{\frac{3}{2}}} & 0 \end{bmatrix} \quad l_x > 0 \tag{65}$$

$$\frac{\partial \boldsymbol{f}_1}{\partial \boldsymbol{f}_2} = \frac{1}{2\sqrt{2}} \begin{bmatrix} 0 & -\frac{2}{\kappa} & -\frac{a_y}{\kappa^3} & 0 & 0 & 0 \\ 0 & 0 & -\frac{1}{\kappa} & 0 & 0 & 0 \\ 0 & 0 & 0 & 0 & 0 & 0 \\ \frac{2}{\kappa} & 0 & \frac{a_x}{\kappa^3} & 0 & 0 & 0 \\ 0 & 0 & 0 & \frac{l_y \beta_2}{\gamma^{\frac{3}{2}}} & -\frac{l_x \beta_2}{\gamma^{\frac{3}{2}}} & 0 \\ 0 & 0 & 0 & 0 & 0 & 0 \\ 0 & 0 & 0 & 0 & 0 & 0 \\ 0 & 0 & 0 & -\frac{l_y^2}{\beta_2 \gamma} & \frac{l_x l_y}{\beta_2 \gamma} & 0 \end{bmatrix} \quad l_x < 0 \tag{66}$$

$$\frac{\partial \boldsymbol{f}_2}{\partial \boldsymbol{u}} = \begin{bmatrix} & \mathbf{I}_{3\times 3} & & & \mathbf{0}_{3\times 3} & \\ m_z - \frac{2a_x m_x + a_y m_y}{\kappa^2} & -\frac{a_x m_y}{\kappa^2} & \frac{a_x(a_x m_x + a_y m_y)}{\kappa^4} & 1 - \frac{a_x^2}{\kappa^2} & -\frac{a_x a_y}{\kappa^2} & a_x \\ -\frac{a_y m_x}{\kappa^2} & m_z - \frac{a_x m_x + 2a_y m_y}{\kappa^2} & \frac{a_y(a_x m_x + a_y m_y)}{\kappa^4} & -\frac{a_x a_y}{\kappa^2} & 1 - \frac{a_y^2}{\kappa^2} & a_y \\ -m_x & -m_y & m_z & -a_x & -a_y & a_z \end{bmatrix} \tag{63}$$

$$\frac{\partial \boldsymbol{f}_2}{\partial \boldsymbol{u}} = \begin{bmatrix} & \mathbf{I}_{3\times 3} & & & \mathbf{0}_{3\times 3} & \\ m_z - \dfrac{2a_x m_x - a_y m_y}{\kappa^2} & \dfrac{a_x m_y}{\kappa^2} & \dfrac{a_x(-a_x m_x + a_y m_y)}{\kappa^4} & 1 - \dfrac{a_x^2}{\kappa^2} & -\dfrac{a_x a_y}{\kappa^2} & ax \\ -\dfrac{a_y m_x}{\kappa^2} & m_z - \dfrac{a_x m_x - 2a_y m_y}{\kappa^2} & \dfrac{a_y(-a_x m_x + a_y m_y)}{\kappa^4} & -\dfrac{a_x a_y}{\kappa^2} & -1 + \dfrac{a_y^2}{\kappa^2} & ay \\ m_x & -m_y & -m_z & a_x & -a_y & -a_z \end{bmatrix} \tag{67}$$

and $(\partial \boldsymbol{f}_2/\partial \boldsymbol{u})$ as per (67), as shown at the top of this page, with $\kappa = (1 - a_z)^{1/2}$ and γ, β_1, and β_2 as previously defined. Note that for convenience, we used the notations q_a and q_m instead of q_{acc} and q_{mag}. Finally, the total Jacobian matrix is obtained by multiplying the three matrices, as per (45), and the covariance matrix of the quaternion orientation through (41).

REFERENCES

[1] T. N. Hung and Y. S. Suh, "Inertial sensor-based two feet motion tracking for gait analysis," *Sensors*, vol. 13, no. 5, pp. 5614–5629, 2013.

[2] V. Renaudin and C. Combettes, "Magnetic, acceleration fields and gyroscope quaternion (MAGYQ)-based attitude estimation with smartphone sensors for indoor pedestrian navigation," *Sensors*, vol. 14, no. 12, pp. 22864–22890, 2014.

[3] J. K. Hall, N. B. Knoebel, and T. W. McLain, "Quaternion attitude estimation for miniature air vehicles using a multiplicative extended Kalman filter," in *Proc. IEEE/ION Position, Location, Navigat. Symp.*, Monterey, CA, USA, May 2008, pp. 1230–1237.

[4] S. Wang and Y. Yang, "Quadrotor aircraft attitude estimation and control based on Kalman filter," in *Proc. 31st Chin. Control Conf.*, Hefei, China, Jul. 2012, pp. 5634–5639.

[5] S. Ayub, A. Bahraminisaan, and B. Honary, "A sensor fusion method for smart phone orientation estimation," in *Proc. 13th Annu. Post Graduate Symp. Converg. Telecommun., Netw., Broadcast.*, Liverpool, U.K., Jun. 2012, pp. 1–6.

[6] J. Goslinski, M. Nowicki, and P. Skrzypczynski, "Performance comparison of EKF-based algorithms for orientation estimation on Android platform," *IEEE Sensors J.*, vol. 15, no. 7, pp. 3781–3792, Jul. 2015.

[7] D. Gebre-Egziabher, R. C. Hayward, and J. D. Powell, "Design of multi-sensor attitude determination systems," *IEEE Trans. Aerosp. Electron. Syst.*, vol. 40, no. 2, pp. 627–649, Apr. 2004.

[8] D. Choukroun, I. Y. Bar-Itzhack, and Y. Oshman, "Novel quaternion Kalman filter," *IEEE Trans. Aerosp. Electron. Syst.*, vol. 42, no. 1, pp. 174–190, Jan. 2004.

[9] J. L. Marins, X. Yun, E. R. Bachmann, R. B. McGhee, and M. J. Zyda, "An extended Kalman filter for quaternion-based orientation estimation using MARG sensors," in *Proc. IEEE/RSJ Int. Conf. Intell. Robots Syst.*, Maui, HI, USA, Oct./Nov. 2001, pp. 2003–2011.

[10] A. M. Sabatini, "Quaternion-based extended Kalman filter for determining orientation by inertial and magnetic sensing," *IEEE Trans. Biomed. Eng.*, vol. 53, no. 7, pp. 1346–1356, Jul. 2006.

[11] H. Zhou and H. Hu, "Reducing drifts in the inertial measurements of wrist and elbow positions," *IEEE Trans. Instrum. Meas.*, vol. 59, no. 3, pp. 575–585, Mar. 2010.

[12] B. Barshan and H. F. Durrant-Whyte, "Inertial navigation systems for mobile robots," *IEEE Trans. Robot. Autom.*, vol. 11, no. 3, pp. 328–342, Jun. 1995.

[13] M. Jun, S. I. Roumeliotis, and G. Sukhatme, "State estimation of an autonomous helicopter using Kalman filtering," in *Proc. IEEE/RSJ Int. Conf. Intell. Robots Syst.*, Gyeongju, Korea, Oct. 1999, pp. 1346–1353.

[14] A.-J. Baerveldt and R. Klang, "A low-cost and low-weight attitude estimation system for an autonomous helicopter," in *Proc. IEEE Int. Conf. Intell. Eng. Syst.*, Budapest, Hungary, Sep. 1997, pp. 391–395.

[15] M. Euston, P. Coote, R. Mahony, J. Kim, and T. Hamel, "A complementary filter for attitude estimation of a fixed-wing UAV," in *Proc. IEEE/RSJ Int. Conf. Intell. Robots Syst.*, Nice, France, Sep. 2008, pp. 340–345.

[16] H. Fourati, N. Manamanni, L. Afilal, and Y. Handrich, "Complementary observer for body segments motion capturing by inertial and magnetic sensors," *IEEE/ASME Trans. Mechatronics*, vol. 19, no. 1, pp. 149–157, Feb. 2014.

[17] S. O. H. Madgwick, A. J. L. Harrison, and A. Vaidyanathan, "Estimation of IMU and MARG orientation using a gradient descent algorithm," in *Proc. IEEE Int. Conf. Rehabil. Robot.*, Zürich, Switzerland, Jun./Jul. 2011, pp. 1–7.

[18] T. S. Yoo, S. K. Hong, H. M. Yoon, and S. Park, "Gain-scheduled complementary filter design for a MEMS based attitude and heading reference system," *Sensors*, vol. 11, no. 4, pp. 3816–3830, 2011.

[19] J. Calusdian, X. Yun, and E. Bachmann, "Adaptive-gain complementary filter of inertial and magnetic data for orientation estimation," in *Proc. IEEE Int. Conf. Robot. Autom.*, Shanghai, China, May 2011, pp. 1916–1922.

[20] Y. Tian, H. Wei, and J. Tan, "An adaptive-gain complementary filter for real-time human motion tracking with MARG sensors in free-living environments," *IEEE Trans. Neural Syst. Rehabil. Eng.*, vol. 21, no. 2, pp. 254–264, Mar. 2013.

[21] J. L. Crassidis, F. L. Markley, and Y. Cheng, "Survey of nonlinear attitude estimation methods," *J. Guid., Control, Dyn.*, vol. 30, no. 1, pp. 12–28, 2007.

[22] L. F. Markley, "Multiplicative vs. additive filtering for spacecraft attitude determination," in *Proc. 6th Int. Conf. Dyn. Control Syst. Struct. Space*, Riomaggiore, Italy, 2004, pp. 467–474.

[23] X. Yun, M. Lizarraga, E. R. Bachmann, and R. B. McGhee, "An improved quaternion-based Kalman filter for real-time tracking of rigid body orientation," in *Proc. IEEE/RSJ Int. Conf. Intell. Robot Syst.*, Las Vegas, NV, USA, Oct. 2003, pp. 1074–1079.

[24] A. M. Sabatini, "Kalman-filter-based orientation determination using inertial/magnetic sensors: Observability analysis and performance evaluation," *Sensors*, vol. 11, no. 10, pp. 9182–9206, 2011.

[25] Z.-Q. Zhang, X.-L. Meng, and J.-K. Wu, "Quaternion-based Kalman filter with vector selection for accurate orientation tracking," *IEEE Trans. Instrum. Meas.*, vol. 61, no. 10, pp. 2817–2824, Oct. 2008.

[26] N. Trawny and S. I. Roumeliotis, "Indirect Kalman filter for 3D attitude estimation," Dept. Comput. Sci. Eng., Univ. Minnesota, Minneapolis, MN, USA, Tech. Rep. 2005-002, 2005.

[27] F. L. Markley, "Attitude estimation or quaternion estimation?" *J. Astron. Sci.*, vol. 52, nos. 1–2, 2004, pp. 221–238.

[28] Y. S. Suh, "Orientation estimation using a quaternion-based indirect Kalman filter with adaptive estimation of external acceleration," *IEEE Trans. Instrum. Meas.*, vol. 59, no. 12, pp. 3296–3305, Dec. 2010.

[29] Y. S. Suh, Y. S. Ro, and H. J. Kang, "Quaternion-based indirect Kalman filter discarding pitch and roll information contained in magnetic sensors," *IEEE Trans. Instrum. Meas.*, vol. 61, no. 6, pp. 1786–1792, Jun. 2012.

[30] G. Wahba, "A least squares estimate of satellite attitude," *SIAM Rev.*, vol. 7, no. 3, p. 409, 1965.

[31] X. Yun and E. R. Bachmann, "Design, implementation, and experimental results of a quaternion-based Kalman filter for human body motion tracking," *IEEE Trans. Robot.*, vol. 22, no. 6, pp. 1216–1227, Dec. 2006.

[32] M. D. Shuster and S. D. Oh, "Three-axis attitude determination from vector observations," *J. Guid., Control, Dyn.*, vol. 4, no. 1, pp. 70–77, 1981.

[33] E.-H. Seo, C.-S. Park, D. Kim, and J.-B. Song, "Quaternion-based orientation estimation with static error reduction," in *Proc. Int. Conf. Mechatronics Autom.*, Beijing, China, Aug. 2011, pp. 1624–1629.

[34] X. Yun, E. R. Bachmann, and R. B. Mcghee, "A simplified quaternion-based algorithm for orientation estimation from earth gravity and magnetic field measurements," *IEEE Trans. Instrum. Meas.*, vol. 57, no. 3, pp. 638–650, Mar. 2008.

[35] W. G. Breckenridge, "Quaternions—Proposed standard conventions," JPL, Pasadena, CA, USA, Tech. Rep. IOM 343-79-1199, 1999.

[36] *NOAA/NCEI the World Magnetic Model*. [Online]. Available: http://www.ngdc.noaa.gov/geomag/WMM/, accessed Mar. 2015.

[37] R. E. Kalman, "A new approach to linear filtering and prediction problems," *J. Basic Eng.*, vol. 82, no. 1, pp. 35–45, 1960.
[38] E. B. Dam, M. Koch, and M. Lillholm, "Quaternions, interpolation and animation," Dept. Comput. Sci., Univ. Copenhagen, Copenhagen, Denmark, Tech. Rep. DIKU-TR-98/5, 1998.
[39] Phidgets Inc. *1056 PhidgetSpatial 3/3/3*. [Online]. Available: http://www.phidgets.com/products.php?product_id=1056, accessed Dec. 2014.

Roberto G. Valenti was born in Catania, Italy. He received the M.S. degree in electronics engineering from the University of Catania, Catania, in 2009. He is currently pursuing the Ph.D. degree with The City College of New York (CUNY), New York, NY, USA.

He joined the Department of Electrical Engineering, CUNY, as a Research Assistant. His current research interests include microaerial-vehicles, modeling, simulation, sensor fusion, and control.

Ivan Dryanovski was born in Sofia, Bulgaria. He received the B.A. degree in physics from Franklin and Marshall College, Lancaster, PA, USA, in 2007, and the M.Sc. degree in computing science from Imperial College London, London, U.K., in 2009. He is currently pursuing the Ph.D. degree in computer science with The Graduate Center, The City University of New York (CUNY), New York, NY, USA.

His current research interests include computer vision, 3-D mapping, simultaneous localization and mapping, and quadrotor MAV systems.

Jizhong Xiao (SM'00) received the B.S. and M.S. degrees from the East China Institute of Technology, Nanjing, China, in 1993 and 1990, respectively, the M.E. degree from Nanyang Technological University, Singapore, in 1999, and the Ph.D. degree from Michigan State University, East Lansing, MI, USA, in 2002.

He started the Robotics Research Program at the City University of New York (CUNY)–City College (CCNY), New York, NY, USA, in 2002, as the Founding Director of the CCNY Robotics Laboratory. He is currently a Professor of Electrical Engineering with CCNY, and a Doctoral Faculty Member of the Ph.D. Program in Computer Science at the CUNY Graduate Center. His current research interests include robotics and control, cyber-physical systems, autonomous navigation and 3-D simultaneous localization and mapping, real-time and embedded computing, assistive technology, multiagent systems, and swarm robotics.